Interpretation of Multi-Aspect High-Resolution Polarimetric SAR images

Dirk Borghys and Christiaan Perneel and Marc Acheroy

Royal Military Academy, Signal & Image Centre, Renaissancelaan 30, B-1000 Brussels, Belgium

ABSTRACT

The aim of this article is to explore new methods to enhance the results of automatic interpretation of SAR images by combining images acquired from different viewing directions (multi-aspect SAR images). Using the combined information extracted from multi-aspect images allows to resolve problems of obscurance, by for instance the borders of a forest, to increase the resolution and to augment the confidence in detection as compared to detection in single images.

The article focuses on high-resolution polarimetric images for the automatic interpretation of an airfield scene. Specifically for this type of images we have developed a set of new image interpretation tools such as edge detectors and bar (line) detectors, both based on multi-variate statistics. These detectors are briefly described in the article. The main part of the proposed article will focus on how the use of multi-aspect images can enhance the results of these detectors. The multi-aspect images are supposed to be accurately registered. It is thus possible to warp them into a common coordinate system. Because the spatial resolution of a SAR system is usually not the same in range and azimuth, it is sometimes better to detect objects in each image separately and fuse the results of the detection at the object level. This is particularly true for the detection and delimitation of the buildings. On the other hand, edge detectors can benefit from combined information on a pixel-level. In particular edge detectors based on multi-variate statistical methods can be applied on registered images, thus increasing the confidence level of detection and reducing the false alarm rate, by combining the information at a low level. For edge detectors we will compare results of combining the information available from multi-aspect polarimetric images at different levels. In particular we will compare the results of applying them directly to the registered image set with these obtained when applying them on each individual image and fusing the results at the object level or intermediate (edge-strength) level. Similar investigations will be presented for the bar detectors. Results will be shown on a set of polarimetric L-band images of an airfield.

Keywords: Multi-Aspect SAR Images, Polarimetric SAR, Edge Detection, Road Detection

1. INTRODUCTION

The aim of this article is to explore new methods to enhance the results of automatic interpretation of SAR images by combining images acquired from different viewing directions (multi-aspect SAR images). The different images are supposed to be accurately registered, e.g. by a method such as proposed in.[1] Combining the information of SAR images acquired from different viewing directions allows to resolve problems of obscurance (in shadow areas) or improve detection performance. In[2] segmentation results of multi-aspect images are combined to reduce the false segmentations in forest shadow areas. In[3] multi-aspect images are used to improve the extraction of the boundaries of buildings from the size of their shadows observed in different directions. The results are further improved in[4, 5] by also incorporating height information from interferometric SAR images. As far as we know the problem of exploiting information from multi-aspect SAR images for improving the results of edge or bar detectors has not yet been treated in literature. This article will therefore focus on this subject. In the aforementioned applications (i.e. reduction of obscurance and building detection) information is extracted from each separate viewing direction and the results are fused at the object-level. For edge and line detection we will investigate the possibility of running the detectors directly on the combined dataset obtained by registering the multi-aspect images. This approach is made possible by using multi-variate statistical methods in the development of the edge and bar detectors.[6] This method is compared with methods where the information from the different viewing

Further author information: Send correspondence to Dirk.Borghys@elec.rma.ac.be

directions is combined at other levels. The current paper focuses on high-resolution polarimetric images and results are shown on a set of L-band E-SAR images. In the next section the image set is described. Section 3 investigates the problem of edge detection and in section 4 a bar detector is built and applied to find roads in the image.

2. OVERVIEW OF THE IMAGE SET

The image set consists of two full-polarimetric L-band images acquired by the E-SAR system of the German Aerospace Agency (DLR). Between the two images the viewing direction was changed by approximately 90^o. In fig. 1 the two ground-range images are shown. From these images it is clear that the spatial resolution in range (horizontal direction) is different from the resolution in azimuth (vertical direction). In fig. 2 a part of both images covering the same region is shown in detail. The second image is rotated by 90^o to facilitate the visual comparison. The aspect ratio was not changed. On the top of the image a railway is visible. At the bottom there are some airfield buildings. Some objects are more clearly distinguished on one image than on the other. This is particularly true for the roads between the airfield buildings.

Figure 1. Polarimetric E-SAR images (HH:Red, HV:Blue, VV:Green)

Figure 2. Part of both images in original scale (image 2 rotated by 90°)

3. EDGE DETECTION IN SAR IMAGES

3.1. Single-aspect mono-polarisation images

Edge detectors that work well in optical images fail in SAR images. This is due to the particular properties of the speckle in SAR images.[7] The most efficient edge detectors for optical images use a gradient-based method, mostly combined with a smoothening filter. These are well adapted for images with additive noise and a high signal-to-noise ratio (SNR). However, the speckle in SAR has the characteristics of a multiplicative noise (in intensity images) with a very low signal-to-noise ratio. This makes pixel-wise methods using a simple filtering mask inappropriate. Even more elaborate local methods using a combination of an edge detection filter with some smoothening[8,9] give very noisy results.

The solution that is commonly adopted is to take into account larger neighbourhoods of each pixel to decide whether an edge passes through that pixel. This is mostly done using the following principle (Fig. 3): the images are scanned by a set of two adjacent rectangular windows and in each pixel local measurements, which are a function of statistical differences between the pixels in both windows, are used as an indication that the edge between the two windows actually corresponds to an edge in the image. This gives an answer for one possible edge orientation. The set of rectangles is rotated around the current pixel to verify the presence of an edge along other orientations. Mostly 2, 4 or 8 different orientations are tested.

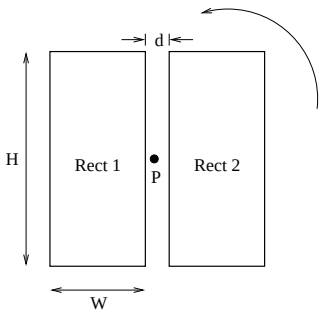

Figure 3. General Principle for Edge Detection in SAR Images

The existing methods were mostly applied on multi-look intensity images and differ by the comparison criterion that is used. An overview is given in.[10] In the same reference an edge detection method is developed for single-look complex images taking into account the spatial correlation in the images.

3.2. Single-aspect full-polarimetric images

A polarimetric SAR image provides a measurement of the scattering matrix in each pixel of the image, i.e. each pixel is characterised by a value for each of the three polarisations HH, HV and VV. An obvious way to detect edges in such multi-channel images is to fuse the results of existing detectors applied on each individual channel but we wished to investigate a way to use the information of all channels in the development of the detector. In particular, we investigated the use of multi-variate statistical methods. For multi-channel data we developed two detectors based on multi-variate hypothesis tests.[6] We also investigated the use of statistical hypothesis tests for edge detection in single-channel SAR images. Fig. 4 illustrates the two approaches that can be used for detecting edges in multi-channel (i.e. polarimetric in this case) SAR images.

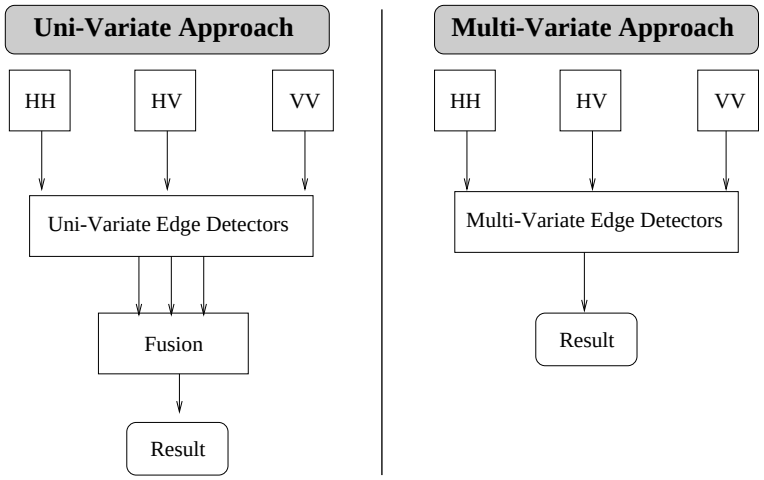

Figure 4. Edge Detection in Polarimetric SAR images

In[6] a Hotellings-T^2 test[11, 12] for the difference in means was applied to single-look log-intensity images and a Levene test[12] for the difference in variance was applied to the single-look complex SAR image. In this article we will use the Hotellings-T^2 test which is briefly described in appendix A. We found that the spatial correlation in the images jeopardizes the CFAR (Constant False Alarm Rate) behaviour of the detectors. The solution proposed in[6] was to use random sub-sampling without replacement in the scanning windows to reduce the spatial correlation. An alternative that turned out to give better results is to sub-sample on a fixed grid (see appendix B).

We have seen that the results obtained by the multi-variate methods are better than those obtained by fusing the outcomes of uni-variate detectors over the three polarisations. This is probably due to the fact that the multi-variate methods use the polarimetric covariance matrix and hence take the full polarimetric information into account.

An existing method for extracting bright bars (lines) and converting them into objects[9] is used to vectorise the results of the edge detectors. The bar detector is applied to the thresholded results of the detector.

3.3. Multi-aspect full-polarimetric images

The problem of edge detection in multi-aspect SAR images can be treated in several ways (see also fig. 5):

1. Detect edges in each separate image, vectorise the results, warp the results onto one image and fuse them (object-level fusion).

2. Detect edges in each separate image, warp the raw results (edge-strength images) onto one image, fuse the edge-strength images and vectorise the result. In this case image-level (low-level) fusion methods can be used.

3. Warp the images onto the coordinate space of a single image and apply the multi-variate edge detectors to the combined information. An equivalent alternative is to warp the elements of the scanning rectangles from one image to the others. In both cases a multi-variate dataset from all images is used as input for the detectors and no supplementary fusion step is needed

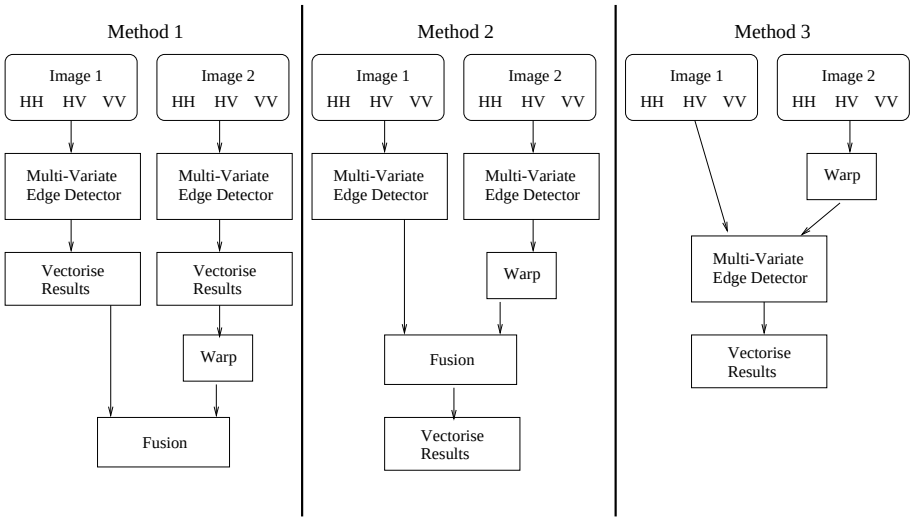

Figure 5. Possible methods for edge detection in multi-aspect images

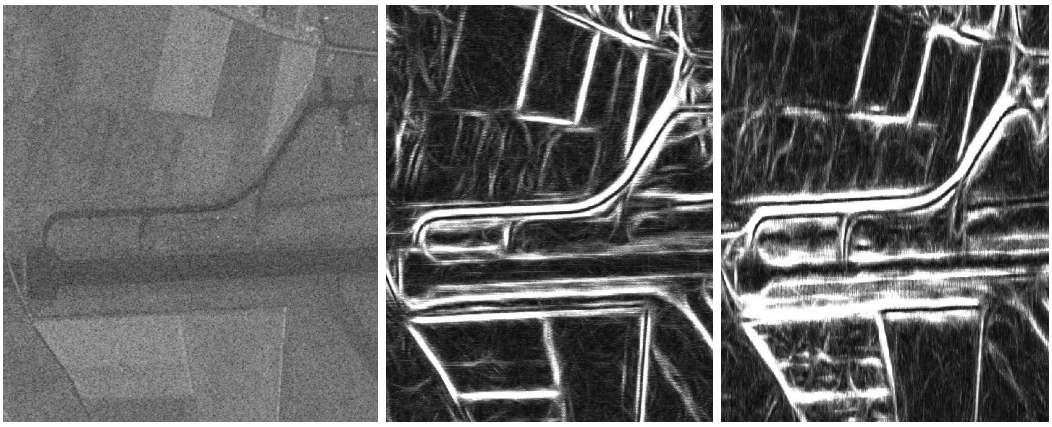

Figure 6. Original image and results of using only image 1 (left) and only image 2 (right)

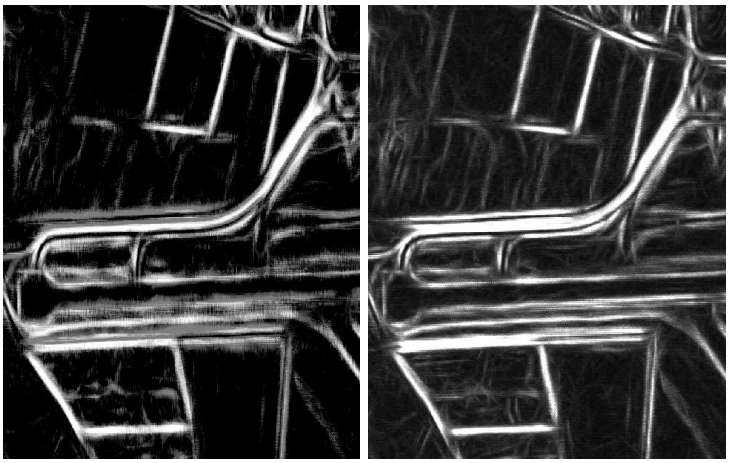

Figure 7. Results of fusion the detector's response from both the separate images (left) and the result of the combined image set (right)

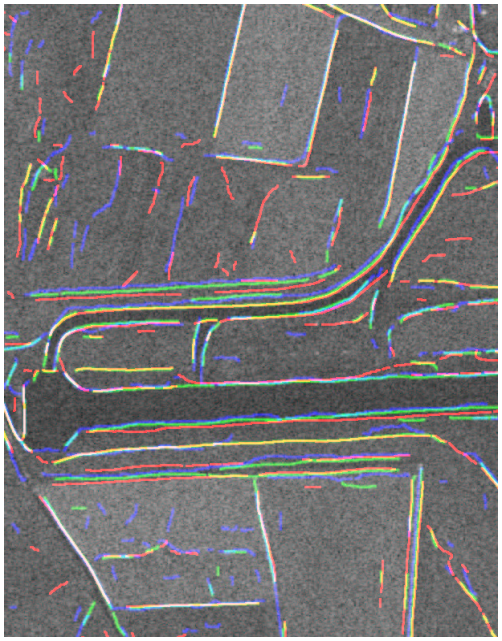

LEGEND:

Color	Img 1	Img 2	Combined Set
	X		
		X	
			X
	X		X
		X	X
	X	X	
	X	X	X

Figure 8. Vectorised results of the edge detection

In fig. 6 the results of the edge detection based on the Hotellings T^2 test, applied on the two separate polarimetric images, are shown. The middle image shows the results obtained in the first image, the right image show the results of the second image, warped into the coordinate space of the first. The left image is the corresponding part of the VV-polarised component image 1. From the figure it seems that the edges detected in image 2 and warped to image 1 are blurred. This is mainly due to the difference in spatial resolution between the horizontal and vertical directions in the image, i.e. the warping compresses the edges from the second image in the horizontal direction and interpolates them in the vertical direction. Several methods to fuse the edge response images (method 2 in fig 5) were tried. The best results were obtained using a non-associative symmetrical sum.[13]

The results of this fusion are shown in the left image of fig. 7. In fig. 7(right) the results of applying the edge detector directly to the combined dataset from both viewing directions (method 3 in fig 5) is shown. Apparently these results are sharper than the results after fusion (fig. 7(left)) and they contain less false alarms than the results of the detector applied to the separate images.

In fig. 8 the vectorised results of the edge detection is shown as color overlays on a part of the first SAR image. The red lines are the vectorised results obtained by applying the detector on image 1 only. The blue lines are the results obtained on image 2 that were warped to image 1. In green the results obtained when the combined image set is used as an input of the detector. The other colors are obtained by mixing the three basic colors. From the figure it seems that the vectorised results from the two images (red and blue lines) do not always coincide. This can be due to the difference in viewing direction (especially for objects with a vertical structure such as fences) to a inaccuracy of the registration or to terrain relief. The different location of the vectorised results would make object-level fusion difficult. Method 1 in fig. 5 is thus discarded. The results obtained using the combined image set are geometrically located between the results for the two separate images. Furthermore some of the false alarms that are visible in the single image results are not seen in the combined result while most of the correct edge structure is detected using the combined set even if it was only detected in one of the single images (cf. cyan and yellow colored lines).

The best results for edge detection are obtained using method 3 in fig 5, i.e. by using the combined dataset available from the two viewing directions.

4. DETECTION OF ROADS

4.1. Single-aspect images

In order to detect roads, a bar detector (bars = narrow lines) was developed. In[14,15] a method for constructing a bar detector for SAR images is presented. The idea is similar to the one that is used for the edge detectors: In order to determine whether a road passes through a given point, in a given direction, a set of rectangles is defined around the point and some statistics are determined in each of the rectangles. The decision is based on a difference between the values of the statistics obtained in the different rectangles. This time three rectangles are used. The middle one is centered on the current point and is narrower than the two others. In fig. 9 the principle is represented schematically.

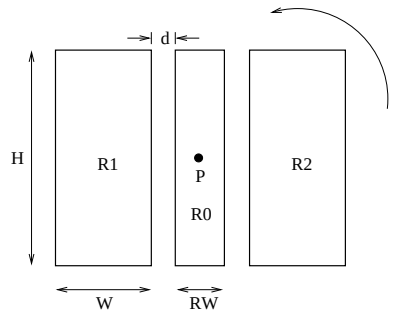

Figure 9. General Principle for Line Detection in SAR Images

In order to detect whether a line in a given orientation passes through the point P the statistics of the two outer rectangles are compared with those in the middle one. The response of the detector is the response corresponding to the smallest difference in statistics. This allows to distinguish edges from lines. The width of the central rectangle has to be chosen such that it corresponds to the possible widths of the lines to be detected. When searching for roads on an image of known spatial resolution sensible boundaries for possible road widths can be set. Furthermore, if the image has already been roughly registered with a map, the information from the map can be used to set these boundaries. The gaps between the middle and outer rectangles not only allow to

reduce the correlation between the three rectangles, but also builds-in a tolerance for the possible widths of the roads.

The surface of road is very smooth compared to the wavelength of the radar. The Rayleigh criterion considers a surface to be smooth if its height variations ΔH fulfill:

$$\Delta H \ll \frac{\lambda}{8cos(\theta)} \tag{1}$$

with λ the wavelength of the radar and θ the local incidence angle. For the E-SAR system the incidence angle varies from 25^o to 57^o over the swath. This yields respectively 3 and 5 cm for the Rayleigh condition in an L-Band image ($\lambda = 23cm$). The surface of the road will thus behave as a mirror. In many cases roads will therefore appear very dark in the SAR image. However, due to the direct environment of the road and in particular the presence of shrubs, trees, ditches boarding the road, double bounce reflections can occur and the road will appear very bright.[15] This effect only occurs for roads that are almost perpendicular to the viewing direction of the radar. Roads will thus either appear very dark or very bright in each of the polarisations. An extra condition in the road detection algorithm can thus be based on a comparison of the average greyvalue of the centre rectangle A_{R_o} with the one found in the two outer rectangles A_{R_1} and A_{R_2}. The response F_T of the detector for dark bars will thus be:

$$\begin{array}{ll} F_T & = MIN(F_{R_o,R_1}, F_{R_o,R_2}) \quad if\ (A_{R_o} < A_{R_1})\ and\ (A_{R_o} < A_{R_2}) \\ & = 0 \qquad\qquad\qquad\qquad\qquad\quad otherwise \end{array} \tag{2}$$

The test-statistic F is defined in appendix A.

4.2. Multi-aspect images

For combining the information from the different viewing directions, the same three possibilities exist as for the detection of edges. The results of the road detection are shown in fig. 10 and fig. 11. In fig. 10 the results obtained by using only image 1 is shown in the middle, on the right the results obtained in image 2 are shown (warped onto image 1 coordinate space), on the left the corresponding part of the original image (VV-polarised component) is shown. Fig. 11(left) shows the results obtained by fusion of the results in fig. 10, i.e. the results of applying method 2 in fig.5. Several fusion methods were tried and the non-associative sum gave the best results. These are shown in the figure. On the right side of fig. 11 the results obtained by applying the road detector on the combined dataset are shown (corresponding to method 3 in fig.5).

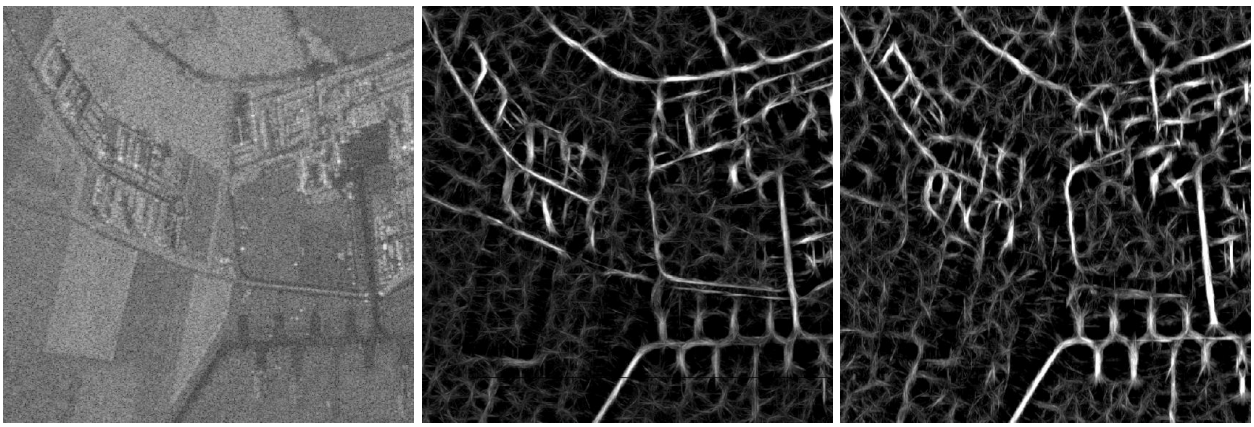

Figure 10. Original image and results of using only image 1 (left) and only image 2 (right)

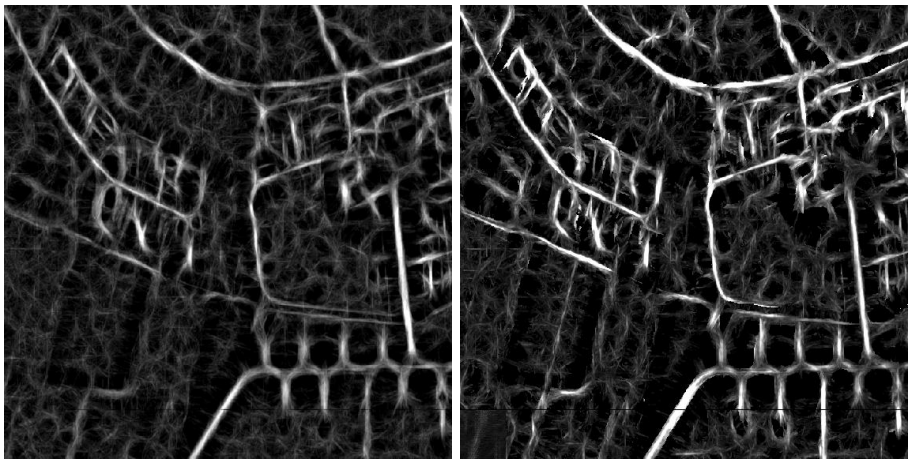

Figure 11. Results of fusion the detector's response from both the separate images (left) and the result of the combined image set (right)

It seems that for road detection the results obtained by directly applying the bar detector to the combined dataset are again slightly better than those obtained by fusion of the results from separate images.

5. CONCLUSIONS AND FURTHER WORK

In this paper we examined ways to improve the detection of edges and linear structures (roads) in polarimetric SAR images by combining information from images acquired from different viewing directions, i.e. multi-aspect images. Several ways to combine the information from multi-aspect images were investigated and compared. It turned out that combining the multi-aspect information at the lowest level, by warping the images in the same coordinate system and applying the detector on the combined dataset provides the best results. Applying the edge and line detectors directly on the combined dataset is facilitated by the fact that both types of detectors are based on multi-variate statistical methods which makes the extension of the input dataset straightforward. Problems are still encountered for the edge detection at the location of shadow areas (e.g. from forest boundaries). Because such shadows appear at different locations in images acquired from different viewing directions, combining the information from multi-aspect images at a low-level results in detection of all of the boundaries of shadows. This is illustrated in fig. 12 where a clearing in a forest is shown. On the left a part of the first image is shown with the corresponding detected edges, in the middle the same region from the second image is shown warped into the coordinate space of the first image, on the right the combined results are shown. The edges corresponding to all shadows are detected. However, if the forests could be detected beforehand, this information could be incorporated into the edge detection methodology to eliminate the forest shadows. This still needs to be investigated.

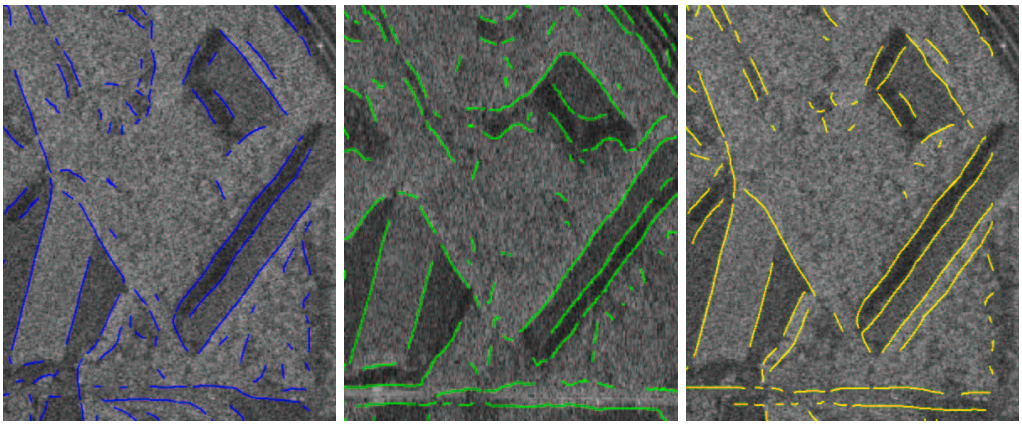

Figure 12. The problem of edge detection in multi-aspect images of forests

On the other hand vertical structure cause the edges seen in the images to be displaced when viewed from different directions. We still need a to find a way to cope with this problem. Due to the different resolution in range and azimuth in the SAR images, roads that are visible in an image acquired from a given viewing direction are not visible in images acquired from other directions. This might suggest that narrow linear features should be detected in each separate image and the results fused afterwards. However, for the images we examined, the road detection using multi-aspect images gives slightly better results when the images are warped into a common coordinate system and the detector is run on the combined dataset. As the difference is only small we feel that this too should be investigated further in order to exclude the possibility that this result is due to a non-optimal fusion and to confirm the obtained result in other images.

ACKNOWLEDGMENTS

The presented work is the result of a collaboration between the Signal & Image Centre of the Belgian Royal Military Academy and the Institut für Hochfrequenztechnik und Radarsysteme of the Deutshes Zentrum für Luft- and Raumfahrt (DLR), who also provided the images. The images used in this project are full-polarimetric L-band SAR images acquired by DLR's E-SAR system.

REFERENCES

1. D. Borghys, C. Perneel, and M. Acheroy, "A hierarchical approach for registration of high-resolution polarimetric sar images," in *SPIE Conference on Image And Signal Processing for Remote Sensing VII; Toulouse*, sept 2001.
2. S. Kuttikkad, R. Meth, and R. Chellappa, "Registration and exploitation of multi-pass airborne synthethic aperture radar images," tech. rep., University of Maryland, Computer Vision Laboratory, Center for Automation Research, April 1997.
3. R. Bolter and F. Leberl, "Shape-from-shadow building reconstruction from multiple view sar images," in *Proc. 24th Workshop of the Australian Assoc. for Pattern Recognition*, pp. 199–206, (Villach, Carinthia), 2000.
4. R. Bolter and F. Leberl, "Detection and reconstruction of buildings from multiple view interferometric sar data," in *Proc. IGARSS*, (Honolulu, Hawai), July 2000.
5. R. Bolter and F. Leberl, "Detection and reconstruction of human scale features from high-resolution interferometric sar data," in *Proc. ICPR*, (Barcelona, Spain), September 2000.
6. D. Borghys, C. Perneel, and M. Acheroy, "Contour detection in high-resolution polarimetric sar images," in *SPIE Conference on SAR Image Analysis,Modelling and Techniques III; Barcelona*, sept 2000.
7. R. Touzi, A. Lopes, and P. Bousquet, "A statistical and geometrical edge detector for sar images," *IEEE-GRS* **26**, pp. 764–773, November 1988.

8. J. Canny, "A computational approach to edge detection," *IEEE-PAMI* **8**, pp. 679–698, November 1986.
9. V. Lacroix and M. Acheroy, "Feature extraction using the constrained gradient," *ISPRS Journal of Photogrammetry & Remote Sensing* **53**, pp. 85–94, April 1998.
10. R. Fjörtoft, *Segmentation d'images radar par detection de contour*. PhD thesis, Institut National Polytechnique de Toulouse, Toulouse, March 1999.
11. T. Anderson, *Introduction to Multivariate Statistical Analysis*, John Wiley & Sons, 1958.
12. B. Manly, ed., *Multivariate Statistical Methods*, Chapman and Hall, 1995.
13. I. Bloch, "Information combination operators for data fusion: A comparative review with classification," *IEEE-SMC(Part A)* **26**, pp. 52–67, January 1996.
14. F. Tupin, H. Maitre, J. Mangin, J. Nicolas, and E. Pechersky, "Detection of linear features in sar images: Application to road network extraction," *IEEE-GRS* **36**, pp. 434–453, March 1998.
15. F. Tupin, *Reconnaissance des Formes et Analyse de Scènes en Imagerie Radar à Ouverture Synthétique*. PhD thesis, ENST, Paris, September 1997.

APPENDIX A. THE HOTELLINGS T^2 TEST

The *Hotellings T^2-statistic* is defined as:

$$T^2 = \frac{n_1 n_2 (\overline{\mathbf{X_1}} - \overline{\mathbf{X_2}})^t \mathbf{C}^{-1} (\overline{\mathbf{X_1}} - \overline{\mathbf{X_2}})}{n1 + n2} \tag{3}$$

with $\overline{\mathbf{X_i}}$ the vector of averages of the values in scanning rectangle i (i=1 or 2) and n_i is the number of observations used in the respective scanning rectangle to estimate the test statistics. Each element of the vector represents the average for one polarisation. $[C]$ is the pooled covariance matrix defined as:

$$\mathbf{C} = \frac{(n_1 - 1)\mathbf{C_1} + (n_2 - 1)\mathbf{C_2}}{n_1 + n_2 - 2} \tag{4}$$

with C_1 and C_2 respectively the polarimetric covariance matrix in the first and second scanning rectangle. The significance of T^2 is determined by using the fact that in the null-hypothesis of equal population means the transformed statistic

$$F = \frac{(n_1 + n_2 - p - 1)T^2}{(n_1 + n_2 - 2)p} \tag{5}$$

follows an F distribution with degrees of freedom p and $(n_1 + n_2 - p - 1)$. p is the number of images that is used For a single polarimetric log-intensity image $p = 3$.

The hypotheses that need to be full-filled in order that this test should be valid are:

- the distribution in both populations to be compared should belong to the same family
- the sample size from both regions should be similar
- the sample size should be sufficiently large ($n_i \geq 30$)

In uniform (non-textured) regions the first condition is full-filled. The second condition is full-filled by construction of the detector, i.e. we pick the same number of pixels from both rectangular windows. The third condition limits the size of the windows or the sampling rate within the windows. The log-intensity image is the best candidate for comparing regions on the basis of this test because differences in radar reflectivity appear in these image purely as variations of means and because the form of the distribution is independent of the radar reflectivity.

APPENDIX B. SUB-SAMPLING ON A FIXED GRID

In the derivation of the test-statistics for the Hotellings-T^2 test (e.g.[11]) the assumption is made that the covariance matrix of the mean is equal to the covariance matrix of the samples divided by the number of observations in the samples. This is only true when the observations are uncorrelated. However, in SAR images neighbouring pixels are correlated. This correlation is partly due to the SAR system itself and partly to texture in the terrain. The spatial correlation causes the behaviour of the detectors based on the Hotellings test to deviate from the theoretical prediction (the test-statistic becomes too large and too many false alarms are found at a given theoretical constant false alarm threshold). The part of the spatial correlation that is due to the SAR system can be modeled and a correction factor can be calculated for the test statistics. However, even a slight terrain texture, again introduces an increased spatial correlation and an increased number of false alarms. A solution is to sub-sample the image. When this is done on a fixed grid, the theoretical constant false alarm thresholds can be derived from the average correlation between points on that grid and when the sampling ratio is low enough slight terrain structures only have a minor influence on the detector. For edge detection we have therefore chosen to sample on a grid such that the average spatial correlation between neighbouring pixels on the grid is below 10 %. In table 1 the average spatial correlation found in uniform regions in a log-intensity L-band E-SAR image is shown. The corresponding grid used in the sampling is shown in fig. 13. Note that sub-sampling is possible when edges between large regions need to be detected because large scanning rectangles can then be used. For road detection, i.e. detection of narrow linear features, the detectors need to be used at their full resolution (taking into account the correction factor) and they will thus give more false alarms in textured areas.

	Range →		
Azimuth ↓	1.0000	0.2599	0.0247
	0.6671	0.2237	0.0260
	0.3019	0.1285	0.0187
	0.1036	0.0543	0.0144
	0.0369	0.0205	0.0173

Table 1. Average spatial correlation for the E-SAR system

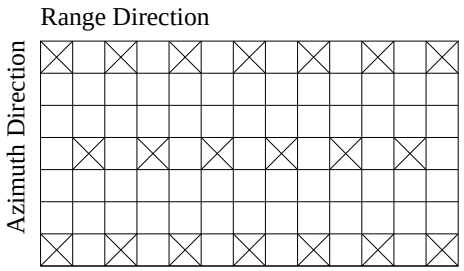

Figure 13. Grid for Fixed Grid Sub-sampling